AIAA JOURNAL
Vol. 35, No. 9, September 1997

Viscous–Inviscid Interaction Using the Navier–Stokes Equations

A. Filippone* and J. N. Sørensen†
Technical University of Denmark, DK-2800 Lyngby, Denmark

A numerical model for the calculation of incompressible viscous flows past airfoils and wings has been developed. The approach is based on a strong viscous–inviscid coupling of a boundary element method with the Navier–Stokes equations in vorticity-stream function formulation. A semiadaptive or fully adaptive grid is used. The interaction is achieved by iterative updating of the boundary conditions, through the wall transpiration concept. The Navier–Stokes equations are discretized on a semistaggered grid. Space-marching integration is performed starting from the stagnation streamline on two independent blocks. Results are presented for two different airfoils. Comparisons with experimental results and other calculations show that the present algorithm performs well for flows at angles of attack up to maximum lift and mild separations.

Nomenclature

$\boldsymbol{A}$, $\boldsymbol{B}$	= boundary element method influence matrix
C_D	= drag coefficient
C_f	= skin-friction coefficient
C_L	= lift coefficient
C_M	= moment coefficient
C_p	= pressure coefficient
$\boldsymbol{D}$	= unit source influence matrix
G	= Green's function
$\boldsymbol{J}$	= Jacobian matrix
k	= curvature
$\mathcal{L}$	= nonlinear operator
M	= Mach number
N	= number of panels
$\boldsymbol{n}$	= unit normal vector
$\boldsymbol{q}$	= velocity vector
r	= distance between two points
s	= arclength
$\boldsymbol{t}$	= unit tangent vector
$\boldsymbol{x}$	= Cartesian coordinates
α	= angle of attack, panel angle
Γ	= circulation
γ	= vortex strength
$\delta*$	= displacement thickness
ϵ	= $1 + \nu/\nu_t$ small quantity
ζ	= vorticity
θ	= momentum thickness
ν	= kinematic viscosity
ν_t	= eddy viscosity
ξ, η	= boundary-fitted coordinate system
σ	= source strength
ϕ	= velocity potential
ψ	= stream function

Subscripts and Superscripts

c	= contravariant
e	= boundary layer edge
I, J	= cell center indices
i	= inviscid
i, j	= cell vertex indices
n	= normal
p	= panel
v	= viscous
$+$	= upper side
$-$	= lower side
∞	= freestream quantity

Received April 10, 1996; revision received May 29, 1997; accepted for publication June 11, 1997.

*Research Associate, Department of Fluid Mechanics. Member AIAA.
†Associate Professor, Department of Fluid Mechanics. Member AIAA.

Introduction

THE viscous–inviscid interaction approach to the calculation of high Reynolds number flows is based on splitting the viscous and inviscid domains and in the formulation of a coupling algorithm, whose solution yields the compatibility of the boundary conditions (BCs) at fixed boundaries. The high Reynolds number assumption alone is not enough to confine the viscous domain in a small region of the wall. This hypothesis must be associated with those of mild pressure gradients (both in the streamwise and normal directions) and limited wall curvature. In this case, two-dimensional airfoil flows currently can be solved using boundary-layer equations and a viscous–inviscid interaction (VII) technique. This approach is recognized as theoretically correct and computationally efficient. Therefore, it usually represents an affordable compromise between numerical complexity and computational cost.

In the past decade some viscous–inviscid techniques have been successfully developed for the prediction of separated turbulent airfoil flows both at low and high Reynolds numbers in incompressible, compressible, transonic, and supercritical regimes. Presently there are three alternatives. Le Balleur's[1] semi-inverse scheme with stability analysis remains a classic robust formulation for airfoil flows. Another method, called quasisimultaneous, originally developed by Veldman[2] and used by Cebeci et al.[3] consists in simultaneously coupling a linear combination of pressure and displacement thickness with the boundary-layer theory. The last alternative is the fully-simultaneous method. It consists in simultaneously solving the inviscid and viscous flow equations, and coupling them through the residuals with a Newton type of iteration.[4]

The viscous–inviscid splitting is valid for the classic boundary-layer equations and the Navier–Stokes equations (NSE) alike.[5] Thus, the VII strategy appears a very general and attractive approach in high Reynolds number aerodynamics.

Some methods that make use of the domain decomposition technique have recently appeared in the literature for the computation of low-speed and compressible oscillating airfoil flows.[6,7] In these works, the integration domain of the NSE encompasses the airfoil in close proximity.

In the VII technique presented in this paper, the viscous flow is modeled by the NSE in vorticity-stream function formulation. The equations are integrated on a semistaggered grid by a space–time marching scheme. BCs are required at the grid outer contour, at the wake centerline, and at the stagnation streamline (found iteratively). These BCs are given through the field of induced velocities computed with the inviscid flow. The viscous–inviscid coupling is performed by iteratively updating the BCs for the viscous and inviscid solver, via a superposition of equivalent inviscid flow (EIF) (Fig. 1). This is a consistent advantage, because there is no need for underrelaxation or for simultaneous viscous and inviscid solutions.

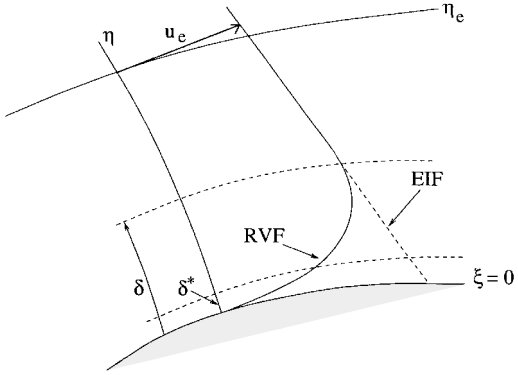

Fig. 1 Overlapping of RVF with EIF for a typical attached boundary layer.

The advantage of employing the NSE in lieu of the boundary-layer equations is that greater generality and higher accuracy can be achieved. Furthermore, the adaptive grid assures that the stagnation streamline and the wake line are a part of the computational mesh; hence, a space-marching procedure is easily performed by integrating the equations from the stagnation line along the main flow direction on either side of the airfoil. The formulation of the NSE in stream function-vorticity variables avoids the problem of explicitly determining the pressure variation across the boundary layer. This choice also facilitates the implementation of the BC, as the vorticity becomes zero on the grid outer contour, as well as along the grid lines defining the stagnation and the wake line.

The inviscid flowfield is modeled by a panel method, and the two solution domains are coupled through a transpiration velocity. Thus, the overall solution proceeds, in principle, as a direct interaction method.

The range of applicability of the model spans from steady flows to unsteady flows at low reduced frequencies and angles of attack just above $C_{L_{\max}}$, beyond which point it becomes increasingly difficult to handle the interaction problem. This approach is specifically designed to be applied to three-dimensional flows.[8]

Potential Flow Model

There are several numerical techniques that can be used with more or less efficiency. Among the less efficient is the vorticity formulation. This class of methods requires at least a first-order integration to obtain results comparable with the velocity potential methods at a given number of panels. Therefore, we will use a velocity potential method to solve the inviscid flow. The total velocity can be expressed as

$$\boldsymbol{q} = \boldsymbol{q}_\infty + \nabla\phi \tag{1}$$

The perturbation potential satisfies the Laplace equation and can be transformed into the following integral boundary equation[9]:

$$\phi^* = -\oint_S \left[\phi\frac{\partial G}{\partial n} - G\frac{\partial \phi}{\partial n}\right] \mathrm{d}S - \oint_{S_w} \Delta\phi \frac{\partial G}{\partial n}\,\mathrm{d}S \tag{2}$$

where S and S_w are the body and wake surfaces, respectively. The wake term is nonzero for unsteady two- and three-dimensional flows. G is the fundamental solution, defined by the equation $\nabla^2 G = \delta(\boldsymbol{x} - \boldsymbol{x}^*)$, where $\delta(\boldsymbol{x} - \boldsymbol{x}^*)$ is the Dirac delta function. The solution of the Dirac equation, with $G \to 0$ as $(\boldsymbol{x} - \boldsymbol{x}^*) \to \infty$ is the point source potential $G = \log(r)/2\pi$. The problem is closed with the condition that

$$\phi^+ = \phi^- = \Delta\phi_w \tag{3}$$

The wake term determines the amount of bound vorticity and, hence, the circulation. Once the equation is solved at the boundary, the velocity field can be computed with the same representation. This can be accomplished by taking the gradient of Eq. (2) with respect to the coordinates of the point $\boldsymbol{x}^*$

$$\boldsymbol{q}^* = -\oint_S \left[\phi\frac{\partial(\nabla G)}{\partial n} - \nabla G\frac{\partial \phi}{\partial n}\right] \mathrm{d}S \tag{4}$$

This equation provides the corresponding velocity influence coefficients used to update the wake. Near the airfoil surface some problems of numerical accuracy can be encountered.

The discretized compact form of Eq. (2) is

$$\boldsymbol{A}\phi = \mathrm{RHS} \tag{5}$$

where RHS is the right-hand side with

$$\mathrm{RHS} = \boldsymbol{B} \cdot \left\{\frac{\partial \phi}{\partial n}\right\} \tag{6}$$

and

$$\boldsymbol{B} = b_{ij} = \oint_S G(\boldsymbol{x}, \boldsymbol{x}_j)\,\mathrm{d}S$$

is the influence matrix depending on the geometry. The solution is found after inversion of the matrix $\boldsymbol{A}$.

Viscous Flow Model

To avoid explicit use of the pressure in the interactive procedure, the vorticity-stream function formulation of the NSE is employed as the viscous flow model. Besides avoiding the problem of pressure–velocity coupling, the advantage of this formulation is that it consists of only one transport equation; hence, going from a full NSE representation to a parabolized or even a boundary-layer approximation is easily accomplished by simple elimination of one or two terms in the equations.

Taking the curl of the momentum equations and using the definitions of stream function and vorticity, we get

$$\frac{\partial \zeta}{\partial t} + \nabla\cdot(\boldsymbol{q}\zeta) = \frac{1}{Re}\nabla^2\left[\left(1 + \frac{\nu_t}{\nu}\right)\zeta\right] \tag{7}$$

and

$$\nabla^2\psi = \zeta \tag{8}$$

where $\boldsymbol{q} = (u, v)$ and ν_t is the eddy viscosity, which is computed with the Baldwin–Lomax turbulence model.[10]

Neglecting the second-order derivatives of the vorticity in the chordwise direction leads to the parabolized NSE. This type of equation is preferred for many practical cases because it can be solved efficiently by using space-marching integration schemes.

Transformation from Cartesian coordinates (x, y) to a boundary-fitted curvilinear mesh is carried out by introducing the general transformation

$$\xi = \xi(x, y), \qquad \eta = \eta(x, y) \tag{9}$$

where (ξ, η) are the coordinates in the curvilinear system. Applying the chain rule of differentiation and after some manipulation, the transformed Eqs. (7) and (8) and are formulated in conservative form as follows:

$$\frac{\partial(J\zeta)}{\partial t} + \nabla\cdot(\boldsymbol{q}^c\zeta) = \frac{1}{Re}\nabla^2\left[\left(1 + \frac{\nu}{\nu_t}\right)\zeta\right] \tag{10}$$

$$\nabla^2\psi = J\zeta \tag{11}$$

where $\boldsymbol{q}^c = (u^c, v^c)$ is the contravariant velocity vector defined as

$$u^c = y_\eta u - x_\eta v, \qquad v^c = -y_\xi u + x_\xi v \tag{12}$$

J is the Jacobian of the transformation, and the Laplacian is defined as

$$\nabla^2 f = \frac{\partial}{\partial\xi}\left[\alpha\frac{\partial f}{\partial\xi} + \gamma\frac{\partial f}{\partial\eta}\right] + \frac{\partial}{\partial\eta}\left[\beta\frac{\partial f}{\partial\eta} + \gamma\frac{\partial f}{\partial\xi}\right] \tag{13}$$

with

$$\alpha = (1/J)(x_\eta^2 + y_\eta^2), \qquad \beta = (1/J)(x_\xi^2 + y_\xi^2)$$
$$\gamma = -(1/J)(y_\eta y_\xi + x_\eta x_\xi) \tag{14}$$

The stream function is now defined as

$$\frac{\partial \psi}{\partial \xi} = v^c, \qquad \frac{\partial \psi}{\partial \eta} = -u^c \tag{15}$$

The viscous flow equations are solved on a C-grid including the viscous flowfield, as well as a part of the inviscid flow domain.

With this choice, BCs for the vorticity are easily established because the vorticity is zero at the grid outer contours and on the grid lines defined by the wake and stagnation line. A Neumann condition is used for the vorticity at the outflow boundary, and at the surface of the airfoil it is determined directly from Eq. (11). At the airfoil surface and along the stagnation and wake lines the stream function is set equal to zero. At the grid outer contour a Neumann condition is employed:

$$\frac{\partial \psi}{\partial \eta} = -u^c_I \tag{16}$$

where u^c_I is determined from the inviscid part of the solution. Likewise, the outflow boundary condition is given as

$$\frac{\partial \psi}{\partial \xi} = v^c_I \tag{17}$$

Numerical Solution

The equations are solved on a body-fitted, staggered C-type grid with the vorticity located on cell centers and the stream function on cell vertices. The staggered grid avoids the need of calculating the vorticity on the solid boundaries and facilitates the determination of the contravariant velocity components [Eq. (15)].

The momentum equation (10) is discretized about the center of each computational cell employing second-order accurate upwinding for the convective terms and central differences for the Laplacian. The discretization of Eq. (13) is carried out by employing central differences about the grid points $C(I, J)$, where I, J denote points at the cell centers:

$$I = i + \tfrac{1}{2}, \qquad J = j + \tfrac{1}{2}$$

The resulting set of equations is solved by the relaxation procedure of Wachspress.[11] Equations (10) and (11) are solved independently of each other as a predictor–corrector scheme, where the momentum equation is employed as the predictor and the Poisson equation for the stream function works as the corrector. Thus, the momentum equation is advanced in time by keeping the stream function fixed from the previous time step, after which the stream function is updated from Eq. (11) with the newly calculated vorticity as the RHS term. The convective terms

$$\nabla \cdot (\boldsymbol{q}^c \zeta) = \frac{\partial (u^c \zeta)}{\partial \xi} + \frac{\partial (v^c \zeta)}{\partial \eta} \tag{18}$$

are treated as follows. In the ξ direction, we use a three-point backward differencing if $u^c_{I,J} \geq 0$ and a three-point forward differencing if $u^c_{I,J} < 0$. The backward differencing is

$$\left[\frac{\partial (u^c \zeta)}{\partial \xi}\right]_{I,J} = \frac{1}{2}\left[3(u^c\zeta)_{I,J} - 4(u^c\zeta)_{I-1,J} + (u^c\zeta)_{I-2,J}\right] \tag{19}$$

The forward differencing is formally the same, with the sign of the terms in Eq. (19) changed.

In the η direction, we use a five-point differencing around the cell center $C(I, J)$ (the indices i and j denote the cell vertices):

$$\left[\frac{\partial (v^c \zeta)}{\partial \eta}\right]_{I,J} = (v^c\zeta)_{I,j+1} - (v^c\zeta)_{I,j} \tag{20}$$

where

$$\zeta_j = \begin{cases} \frac{1}{2}[3\zeta_J - \zeta_{J-1}] & \text{if} \quad v^c_j \geq 0 \\ \frac{1}{2}[3\zeta_J - \zeta_{J-1}] & \text{if} \quad v^c_j < 0 \end{cases} \tag{21}$$

$$\zeta_{j+1} = \begin{cases} \frac{1}{2}[3\zeta_J - \zeta_{J-1}] & \text{if} \quad v^c_{j+1} \geq 0 \\ \frac{1}{2}[3\zeta_{J+1} - \zeta_{J+2}] & \text{if} \quad v^c_{j+1} < 0 \end{cases} \tag{22}$$

This is known as the MUSCL scheme, which is a second-order accurate upwinding scheme. Finally, for the time term we use an Euler implicit scheme:

$$\frac{\partial \zeta}{\partial t} = \mathcal{L}(\zeta) \tag{23}$$

$$\frac{\zeta^{n+1} - \zeta^n}{\Delta t} = \mathcal{L}^{n+1}(\zeta^{n+1}) \tag{24}$$

$$\zeta^{n+1} = \zeta^n + \Delta t\, \mathcal{L}^{n+1}(\zeta^{n+1}) \tag{25}$$

The momentum equation is solved along an η line while marching in the ξ direction. Because each node j is coupled with its two neighbors, this scheme results in a set of tridiagonal systems.

VII

The fundamental concept used to couple viscous and inviscid solutions is the equivalent inviscid flow. A distribution of singularities has to be computed from the wall transpiration concept. The solution of the overall problem requires one additional equation that is an explicit condition of unique pressure at the trailing edge. The converged surface pressure distribution is computed from the VII solution at the boundary-layer displacement surface.

The tools for deriving the characteristics of the viscous layer are the conservation equations (continuity and momentum equation). A general presentation can be derived from the defect formulation,[1] which is an extension of Lighthill's[12] method. For this purpose we consider the viscous and inviscid flows as fully overlapping (Fig. 1). The inviscid flow extending in the viscous region, real viscous flow (RVF), will be called EIF. We define the displacement thickness δ^* as the distance measured along local normal $\boldsymbol{n}$ to the airfoil/wake surface:

$$\delta^* = \frac{1}{\boldsymbol{q}_{iw} \cdot \boldsymbol{t}_w} \int_0^{\eta_e} (\boldsymbol{q}_i - \boldsymbol{q}) \cdot \boldsymbol{t}_w \, d\eta \tag{26}$$

where the subscript iw denotes the inviscid quantity at the wall. The integral term in Eq. (26) is the mass flow defect due to the decelerating effects of the viscous flow. Unfortunately, this definition breaks down in the neighborhood of the stagnation point, where numerically $\delta^* \longrightarrow \infty$ as $u_{iw} \longrightarrow 0$. Because the flow is laminar there, we can use the Falkner–Skan transformation to find an estimate of δ^*.

Integration of the defect equation in the EIF with the BC $\boldsymbol{q}_i = \boldsymbol{q}$ at $\eta = \eta_e$ and $\boldsymbol{q} = 0$ at $\eta = 0$ yields

$$v_{iw} = \frac{\partial}{\partial s}(u_{iw}\delta^*) \tag{27}$$

where v_{iw} is the transpiration velocity at the wall.

The momentum thickness θ is calculated by integrating the momentum equation in the normal direction:

$$\theta = \frac{1}{\|\boldsymbol{q}_e \cdot \boldsymbol{t}_w\|^2} \int_0^{\eta_e} \boldsymbol{q} \cdot \boldsymbol{t}_w (\boldsymbol{q}_e - \boldsymbol{q}) \cdot \boldsymbol{t}_w \, d\eta \tag{28}$$

The use of the NSE leads to some problems related to the calculation of the displacement thickness and the other boundary-layer quantities already defined. These problems are 1) determination of the boundary-layer edge index in the grid $j_e(i)$, 2) numerical inaccuracy at stagnation points, and 3) order of integration.

Critical zones for computing the index $j = j_e$ are the stagnation point and the trailing edge. Generally, the index $j_e(i)$ is not regular. Thus, a two-point backward–forward low-pass Savisky–Golay filter is applied.[13] We assume as the edge of the boundary layer the grid point corresponding to a vorticity $\zeta < \epsilon$, with $\epsilon \sim O(10^{-2})$. If the grid becomes too coarse in the normal direction, the displacement thickness falls between two points. This gives rise to a nonsmooth function.

Around the stagnation point the difference $\boldsymbol{q}_i - \boldsymbol{q}$ is large; therefore, integration of the velocity distribution from Eq. (26) is critical. To avoid this difficulty, a laminar Falkner–Skan profile[14] is used for about 2–4% on either side.

Equation (26) is formally very accurate. However, due to the different nature of the viscous and inviscid solutions, the velocity profiles sometimes show a mismatch, so that it is necessary to use a first-order integration in which $u_i = \text{const} = u_i[j_e(i)]$.

If the flow shows massive separation the difficulties just mentioned become critical. Numerically, it becomes impossible to update the BC.

For a VII solution a problem arises when computing the resulting pressure distribution. Outside the viscous layer we have $C_p = C_{p_i}$, whereas the pressure difference in the RVF and EIF increases in the boundary layer and assumes a maximum at the wall. The reason for this difference lies in the presence of normal pressure gradients and the streamline curvature. It has been proven that

$$C_{p_e} - C_{p_w} = \Delta C_p \sim k(\theta + \delta^*) \tag{29}$$

where k is the local curvature of the displacement surface.[15] Also, the pressure at the wall in the RVF is approximately equal to the pressure at $\eta = \theta + \delta^*$ in the EIF. This turns out to be useful because the final pressure distribution on the airfoil/wake can be computed from the EIF once θ and δ^* are known.

The displacement effect that takes place on the wake is similar to that on a solid wall. Some jumps arise, due to the viscous effects. Considering as positive a normal coordinate pointing upward, the jump in the normal velocity is

$$\Delta v_{iw} = \frac{\partial}{\partial s}\left[(u_{iw}\delta^*)^+ - (u_{iw}\delta^*)^-\right] \tag{30}$$

and the jump in the tangential velocity is

$$\Delta u_{iw} = \left[u_i k(\theta + \delta^*)\right]^- - \left[u_i k(\theta + \delta^*)\right]^+ \tag{31}$$

The latter equation is, in fact, an additional vortex term on the wake due to the wake curvature, which reduces the circulation. This term has to be taken into account, at least in highly asymmetric flows.

Equations (30) and (31) do not ensure unique pressure at the trailing edge for the EIF. Because these jumps must vanish far downstream, the Kutta condition is recovered only in the far wake. At the trailing edge proper, there is a pressure gap, due to normal pressure gradients in the viscous layer. Unique pressure at the trailing edge is recovered at each iteration by forcing an explicit Kutta condition that takes into account the viscous effects. At a given VII sweep, we have a residual

$$\Delta C_p = C_p^+ - C_p^- \tag{32}$$

where the superscripts + and − denote two points on the upper and lower displacement surface ($\theta + \delta^*$), respectively. These two points are part of the solution. Equation (32) implies that there is a vortex $\Delta\gamma_{te}$ concentrated at the trailing edge that adjusts the circulation to a lower value. The relationship between the vortex strength $\Delta\gamma_{te}$ and the pressure gap ΔC_p at the trailing edge is a nonlinear one. The physical solution has to be positive; therefore, one can bracket the interval containing $\Delta C_p = 0$. Because the gradient of this function is not known [with the gradient $\partial(\Delta C_p)/\partial(\Delta\gamma)$, it would be possible to construct a Newton–Raphson method], the problem is solved iteratively using the Wijngaarden–Brent inverse parabolic method.[13] The residual of Eq. (32) is associated to an additional vortex $\Delta\gamma_{te}$ such that

$$\phi_1 - \phi_N + \Delta\phi_w = \Delta\gamma_{te} \tag{33}$$

Equation (33) is assumed to be the last equation of the system equation (5). The advantage of this approach is that only the BC at the trailing edge is updated, whereas the matrix $\boldsymbol{A}$ is inverted only once and stored for the interactive procedure. At the first sweep, when there is no viscous effect, $\Delta\gamma_{te} = 0$ and $\mathrm{RHS}_N = 0$. At the successive sweeps, we set $\mathrm{RHS}_N = \Delta\gamma_{te}$. The algorithm is very fast and converges in six to seven iterations. Other authors, for example, see Ref. 16, minimize the residual ΔC_p [Eq. (32)] at the trailing edge, rather than between two appropriate field points.

EIF

The influence of the viscous flow is added to the inviscid solution through the EIF. A summary of the BC is shown in Fig. 2. Because the airfoil geometry and the wake shape are known, we can construct the unit source influence coefficients $\boldsymbol{D} = d_{jk}$. If the grid is fixed, this calculation is performed only once, and the matrix $\boldsymbol{D}$ is stored for the VII.

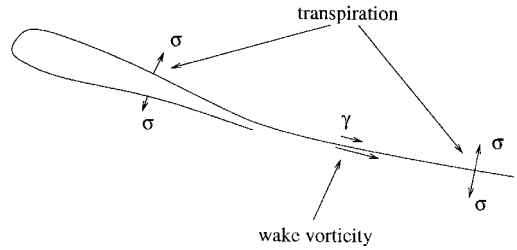

Fig. 2 Summary of boundary conditions for the EIF.

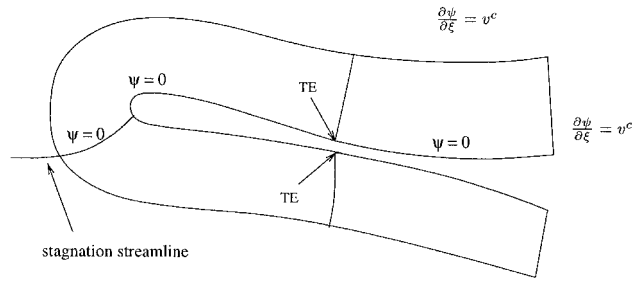

Fig. 3 NSE integration domain and summary of BCs.

The wake centerline is an overlay of two limiting grid lines. To avoid ill conditioning, we consider only the nondoubled points (the full matrix would be N_w times singular), that is, the wake points are counted only once, and the corresponding source will be computed from the jump in the normal velocity $\Delta v_n = v_{iw}^+ - v_{iw}^-$. The total number of node points is $N = N_b + N_w$, and the number of panels is $N - 1$. Considering a constant strength source distribution, we compute the velocity induced by the panel j at the control point of panel k. The influence coefficient d_{jk} is the velocity component normal to the surface; therefore,

$$d_{jk} = \{u, v\}_{jk} \cdot \boldsymbol{n}_k \tag{34}$$

In the panel coordinate system, the induced velocity is

$$u_p = (\sigma/2\pi)\ln(r_1^2/r_2^2), \qquad v_p = (\sigma/2\pi)(\theta_2 - \theta_1) \tag{35}$$

From here a transformation into global coordinates is performed. The induction of a panel on itself yields $u_p = 0$, $v_p = \sigma/2$, and, hence, $d_{jj} = \frac{1}{2}$. For a given distribution of transpiration velocity $\boldsymbol{v}_{iw}$, we can solve the EIF from

$$\sigma = \boldsymbol{D}^{-1}\boldsymbol{v}_{iw} \tag{36}$$

where σ is the corresponding source distribution on the airfoil + wake. The wake curvature effects are recovered with the vorticity distribution given by Eq. (31):

$$\gamma_j = -2\Delta u_{iw}(j) \tag{37}$$

This effect can be neglected for all of the cases where the pressure gradients are mild, but, in general, it has be taken into account for flows approaching rear separation.

We consider a linear distribution of σ and γ over each airfoil/wake panel. The linear distribution is required to remove the logarithmic singularity near the surface. However, if the field point falls too close to a panel, problems of accuracy can be encountered. This happens when the distance of the field point is $O(10^{-4})$ chords or less, which is the size of the first cell of the turbulent Navier–Stokes mesh. Therefore, interpolation is used.

Interactive Procedure

A C-grid is built around the airfoil section. A hyperbolic mesh is generated on the basis of a previous potential flow solution (which needs an estimate of the angle of attack). The integration domain is rendered single-connected considering the trailing-edge stagnation streamline as a solid boundary. After computing the leading-edge stagnation line (via backward fourth-order Runge–Kutta integration), the nose region is modified to match one η line with the stagnation streamline. Now the integration domain consists of two blocks (Fig. 3).

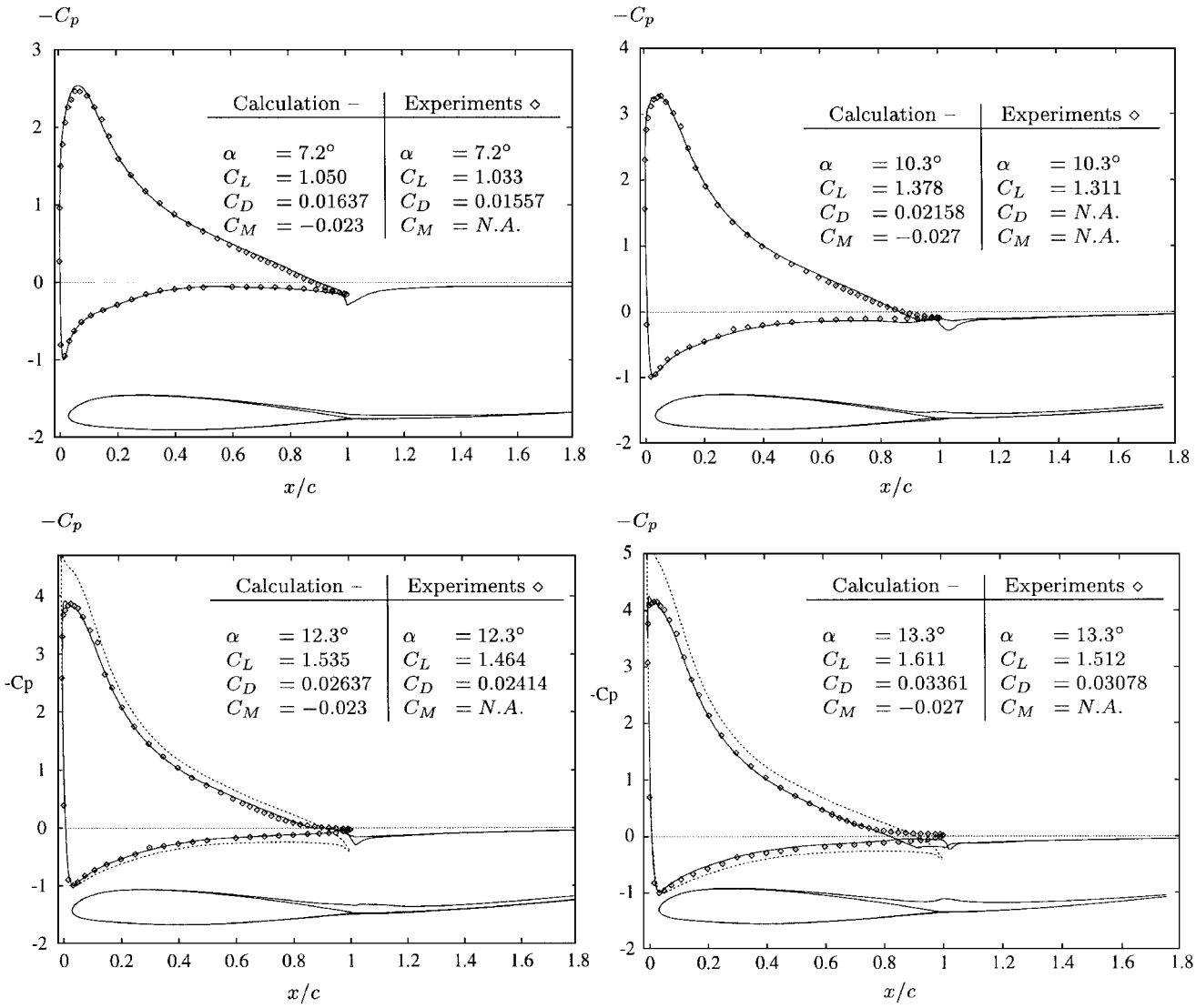

Fig. 4 Computed VII pressure distribution vs experimental results for the airfoil Aérospatiale-A, $Re = 2 \times 10^6$ and $M = 0.15$; dotted line denotes inviscid solution.

With the parabolized NSE, a semiadaptive grid is recommended because the BC must be satisfied exactly on the dividing streamline. This streamline changes position as the interactive calculation proceeds. Wake correction is needed at high angles of attack. The trailing-edge stagnation streamline may change the sign of its curvature in a neighborhood of the trailing edge and presents some problems in the automatic updating.

With the computation of the velocity $\boldsymbol{q} = \{u, v\}$ at the grid points from Eq. (4), BCs are provided to the parabolized NSE. The angle of attack is given implicitly through the field of induced velocity. The interactive procedure consists of the following steps.

1) Solve the inviscid flow with the boundary element method (BEM) algorithm.

2) Solve the viscous flow with the NSE algorithm.

3) Solve the EIF with the EIF algorithm.

4) Iterate between points 2 and 3.

The solution of the EIF requires evaluation of the integral given by Eq. (26), a differentiation [Eq. (27)], and the calculation and inversion of the matrix $\boldsymbol{D}$. Application of the explicit Kutta condition requires calculation of the momentum thickness [Eq. (28)].

The iteration of points 2 and 3 is an outer loop because the EIF is solved after the NSE has run for a number of time steps (typically, 100). At the start of the solution process we use the stream function ψ_i from the BEM as a first guess for the NSE solver. To speed up the convergence, the values of eddy viscosity and vorticity are stored during the interactive procedure and retrieved at the beginning of each NSE solution.

Results

Different airfoils have been studied for the development and validation of the two-dimensional VII. The results are described in this section.

Aérospatiale-A Airfoil

For this airfoil, experimental data are widely available. Moreover, this airfoil has been object of extensive computational fluid dynamics investigation, aimed at developing NSE with suitable turbulence models.[17–19] This extensive testing provides a means to test the present computational method as well as existing full NSE calculations. Other calculations performed with interactive boundary-layer theory showed that the results are quite sensitive to the turbulence model used.

The computations were performed on grids with sizes ranging from (165×37), for the simplest case, to (261×43), for the airfoil approaching stall and beyond. The height in the normal direction was 0.1–0.4 chords. The BCs were updated when the residual decreased by a factor 10^3–10^4. A total of 3–4 VII sweeps was used, corresponding to a total of 500 NSE iterations. Total computing time was about 15 min/operation point on an SGI Indigo 2 computer.

The relevant experimental data were $Re = 2 \times 10^6$ and $M = 0.15$. Turbulent transition was always tripped, as in the results of ONERA.[17] These experiments consist of two different sets ($F1$ and $F2$), which are not in agreement, especially beyond $C_{L_{\max}}$. For

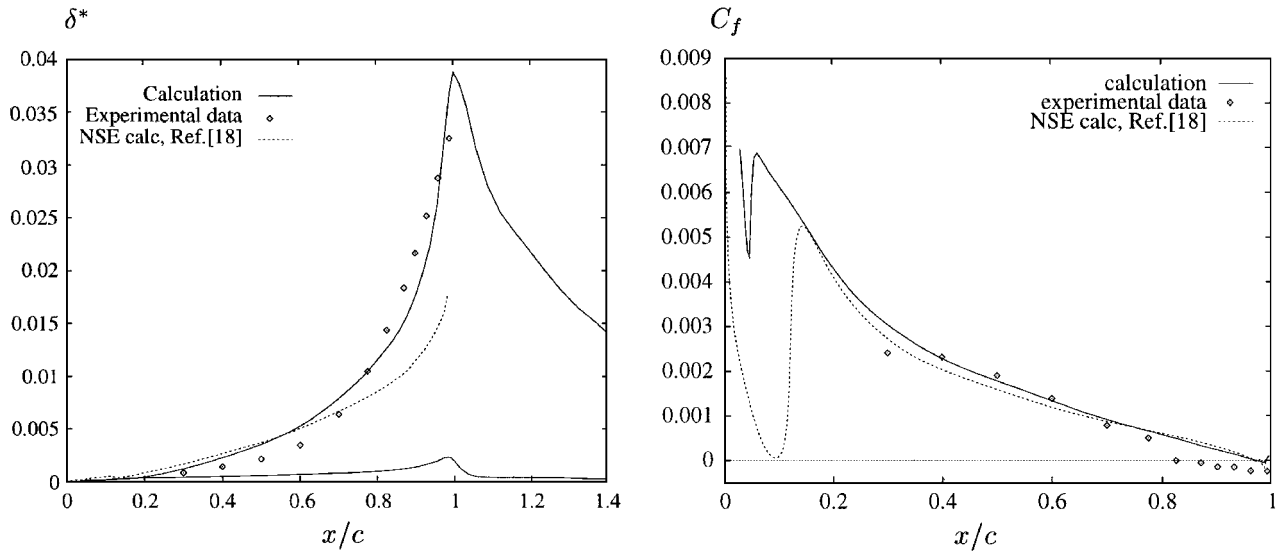

Fig. 5 Aérospatiale-A airfoil at $Re = 2 \times 10^6$, $M = 0.15$, and $\alpha = 13.3$ deg; boundary-layer parameters; VII computations vs experimental results and other full NSE calculation[18] (skin-friction data refer to the suction side of the airfoil).

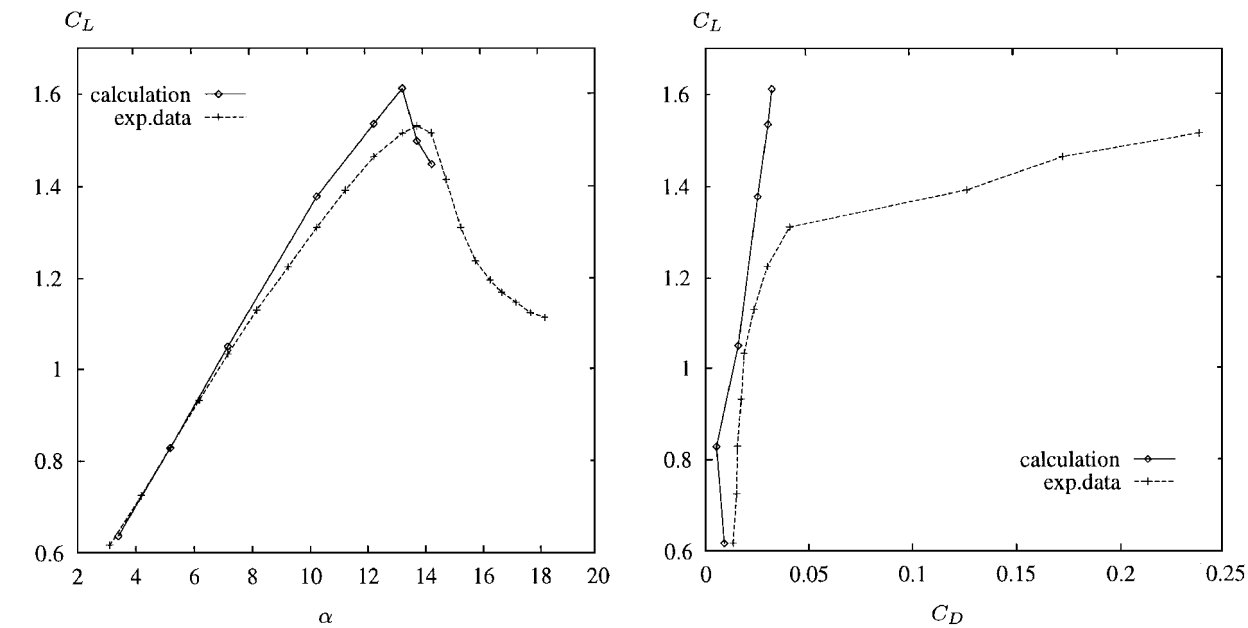

Fig. 6 Polar calculation for the airfoil Aérospatiale-A; lift decrease above $\alpha = 13$ deg is not due to the extent of the separated area but to a strong trailing-edge vortex due to the viscous Kutta condition.

example, at $\alpha = 13.3$ deg, the experimental data are $C_L(F1) = 1.56$ and $C_L(F2) = 1.52$; at $\alpha = 15.3$ deg, the experimental data are $C_L(F1) = 1.67$ and $C_L(F2) = 1.29$. This discrepancy could be explained from the fact that the flow shows a massive rear separation, that is typical of unsteady flows.

At angle of attack $\alpha = 3.1$ deg, the results $F2$ give a C_L higher than a pure inviscid calculation. A correction in the angle of attack to $\alpha = 3.4$ deg (corresponding to the data of the experiment $F1$) was performed in our calculations.

Figure 4 shows the final pressure distribution. The final C_p is denoted by a solid line, the inviscid calculation (where shown) by a dotted line, and the experimental data by dots. A table in the upper-right corner gives the run data. At the bottom of the graph the airfoil with the final wake centerline and the displacement surface is shown. Figure 5 shows the computed displacement thickness and skin-friction distributions compared to the experimental data and the calculations of Ref. 18.

Our numerical model is able to compute flows accurately at moderate angles of attack. The region around $C_{L_{max}}$ is less accurate, and flows with a massive separation could not be computed. The present results, therefore, are in agreement with most NSE computations. The turbulence model (Baldwin–Lomax) could be responsible for the inaccurate velocity profiles. Our polar calculation is shown in Fig. 6.

NACA 0012 Airfoil

The NACA 0012 airfoil, as the Aérospatiale-A, has been the object of extensive experimental and numerical investigation. Calculations done with both VII and thin-layer NSE[20] proved that the determination of the exact turbulent transition is essential for detailed computations. Our model does not incorporate transition modeling.

Calculations have been performed using a grid size ranging from (189×37) to (253×43), with a size in the normal direction of the grid of 0.15–0.35 chords. Comparisons with the experimental results are rather good. The computed pressure distribution is shown in Fig. 7 for angles of attack from 6.0 to 14.0. At the Reynolds number tested, the airfoil does not stall before $\alpha = 16$ deg. The falloff of the C_L after $\alpha = 12$ deg is due to the same circumstances described for the airfoil Aérospatiale-A.

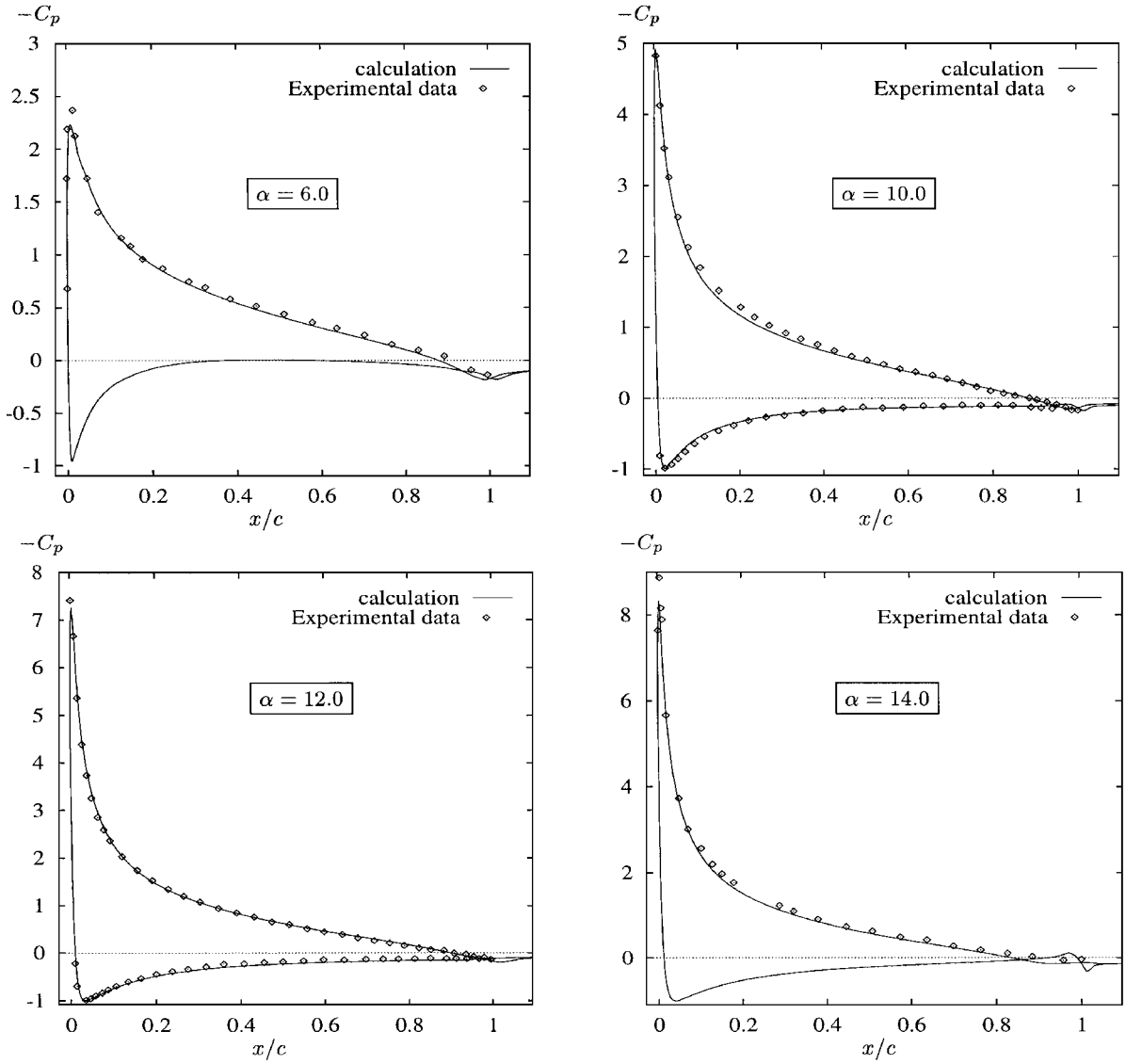

Fig. 7 Computed VII pressure distribution vs experimental results for the airfoil NACA 0012 at $Re = 2.88 \times 10^6$ and $M = 0.1$; turbulent transition fixed as in the experimental data.

Conclusions

A general viscous–inviscid coupling technique was developed under the assumption that the viscous and inviscid equations form a well-posed mathematical problem. The idea is straightforward: solve the viscous and inviscid equations and couple them through updated BCs at boundaries that are part of the solution.

The method is quite general and can be used for the solution of three-dimensionalas well as unsteady flows. The angle of attack is needed as only a first guess.

A very limited number of iterations is required by the VII technique, typically, three to four sweeps. The results are satisfactory for attached and mildly separated flows. The accuracy is at the same level as the current full Navier–Stokes models.

On the other hand, the following has been found.

1) Some limitations in validating the VII are due to the difficulties in correctly computing the new BCs, namely, the blowing velocity and the displacement quantities. (The blowing velocity is the derivative of a nonsmooth function.)

2) A full adaptive grid is needed, at least in those cases that have proven to be the most difficult to compute, that is, near $C_{L_{\max}}$ and beyond.

Acknowledgments

This work was partially supported by Centro Italiano Ricerche Aerospaziali of Italy spa (Contract 930724/01). The authors wish to thank P. Renzoni and A. Visingardi for their valuable comments.

References

[1]Le Balleur, J. C., "Couplage Visqueux-Non Visqueux: Méthode Numérique et Applications aux écoulements Bidimensionnels Transsoniques," *La Recherche Aerospatiale*, Vol. 1978-2, 1978, pp. 65–76.

[2]Veldman, A. P., "New Quasi-Simultaneous Method to Calculate Interacting Boundary Layers," *AIAA Journal*, Vol. 19, No. 1, 1981, pp. 79–85.

[3]Cebeci, T., Clarck, R. W., Chang, K. C., and Halsey, N. D., "Airfoils with Separation and Resulting Wakes," *Journal of Fluid Mechanics*, Vol. 163, Feb. 1986, pp. 323–347.

[4]Drela, M., and Giles, M. B., "Viscous–Inviscid Analysis of Transonic and Low Reynolds Number Airfoils," *AIAA Journal*, Vol. 25, No. 10, 1987, pp. 1347–1355.

[5]Le Balleur, J. C., "New Possibilities of Viscous–Inviscid Numerical Techniques for Solving Viscous Flow Equations with Massive Separation," *Proceedings of 4th Symposium on Numerical and Physical Aspects of Aerodynamic Flows* (Long Beach, CA), Springer–Verlag, 1990.

[6]Ekaterinaris, J. A., Cricelli, A. S., and Platzer, M. F., "A Zonal Method for Unsteady, Viscous, Compressible Airfoil Flows," *Journal of Fluids and Structures*, Vol. 8, Aug. 1994, pp. 107–123.

[7]Tuncer, I. H., Ekaterinaris, J. A., and Platzer, M. F., "Viscous–Inviscid Interaction Method for Unsteady Low-Speed Airfoil Flows," *AIAA Journal*, Vol. 33, No. 1, 1995, pp. 151–154.

[8]Filippone, A., "Interaction of Potential Flow Model with the Navier–Stokes Equations for Rotor Aerodynamics," Ph.D. Thesis, Dept. of Fluid Mechanics, Rept. AFM 95-07, Technical Univ. of Denmark, Lyngby, Denmark, Nov. 1995.

[9]Morino, L., and Kuo, C. C., "Subsonic Potential Aerodynamics for Complex Configurations: A General Theory," *AIAA Journal*, Vol. 12, No. 2, 1974, pp. 191–197.

[10]Baldwin, B. S., and Lomax, H., "Thin Layer Approximation and Algebraic Model for Separated Turbulent Flows," AIAA Paper 78-257, Jan. 1978.

[11]Wachspress, E. L., *Iterative Solutions of Elliptic Systems*, Prentice–Hall, Englewood Cliffs, NJ, 1966, Chap. 4.

[12]Lighthill, M. J., "On Displacement Thickness," *Journal of Fluid Mechanics*, Vol. 4, Aug. 1958, pp. 353–392.

[13]Press, W. H., et al., *Numerical Recipes*, Cambridge Univ. Press, New York, 1992.

[14]White, F., *Viscous Fluid Flow*, McGraw–Hill, New York, 1974, Chap. 3.

[15]Lock, R. C., "A Review of Methods for Predicting Viscous Effects on Airfoils and Wings at Tansonic Speeds," *Computation of Viscous–Inviscid Interactions*, AGARD CP-291, 1981, pp. 2-1–2-32.

[16]Arnold, F., and Thiele, F., "Laplace Interaction Law for the Computation of Viscous Airfoil Flow in Low- and High-Speed Aerodynamics," *AIAA Journal*, Vol. 31, No. 11, 1994, pp. 2178–2185.

[17]Kourta, A., "Maximum Lift Investigation for A-Airfoil," *EUROVAL—A European Initiative on Validation of CFD Codes*, Notes on Numerical Fluid Mechanics, Vol. 42, Viewig, Braunschweig, Germany, 1992.

[18]Sørensen, J. N., Michelsen, J. A., Hansen, M. O. L., Nygreen, P., and Sørensen, D. N., "Incompressible Navier–Stokes Models for Aerodynamics Flows," *Advances in Fluid Mechanics* (to be published).

[19]Chevalier, G., Houdeville, R., and Cousteix, J., "Prévision du Décronage d'un Profil d'Aile par Résolution des Équations de Navier–Stokes Moyennées," *La Recherche Aérospatiale*, Vol. 1995-4, 1995, pp. 277–294.

[20]Mehta, U., Chang, K. C., and Cebeci, T., "Relative Advantages of Thin-Layer Navier–Stokes and Interactive Boundary Layer Procedures," NASA TM-86778, 1985.

D. S. McRae
Associate Editor